Exploring Charge Dissociation by Statistical Sample of Active Layer Models of Organic Solar Cell

Zhi-Wen Zhao,[a,b] Alessandro Troisi,[b] Yun Geng,*[a] Xiao-Fei Wang,*[c] and Zhong-Min Su[a]

[a]Institute of Functional Material Chemistry, Faculty of Chemistry, Northeast Normal University, Changchun, 130024, Jilin, P. R. China. E-mail: gengy575@nenu.edu.cn;

[b]Department of Chemistry, University of Liverpool, Liverpool, L69 3BX, UK.

[c]Key Laboratory for Applied Statistics of MOE and School of Mathematics and Statistics, Northeast Normal Unive rsity, Changchun, 130024, Jilin, P. R. China. E-mail: wangxf341@nenu.edu.cn

ABSTRACT:

Charge dissociation in active layer is one of the key factors for the power conversion efficiency of bulk heterojunction organic solar cells (OSCs). Numerous charge-transfer mechanisms have been proposed based on one of few microscopic models. Here, we would explore possible charge-transfer mechanisms for 155 models of donor/acceptor (D/A) interfaces, built via materials **Dcv-1** and **C_{60}** as donor and acceptor, respectively. After the calculations of the key parameters related to the charge dissociation and a statistical analysis for the correlation between these parameters were carried out, we can obtain a more robust description of the charge dissociation in practical OSCs. The complicated relationship among the key parameters not only illustrates the important correlation between D/A stacking pattern and charge-transfer mechanism, but also suggests that different charge-transfer mechanisms become more likely depending on the specific arrangements of donor and acceptor. Furthermore, the effects of excess energy on the charge-transfer mechanism were preliminarily probed by quantum dynamics simulation, which helps clarifying the much debated role of excess energy on the efficiency of charge generation.

Bulk heterojunction (BHJ) organic solar cells (OSCs) have been developed with continuous breakthrough of efficiency record in OSCs since the initial report in 1995.[1] In recent years, OSCs have obtained considerable attention by virtue of their distinctive superiorities.[2, 3] As the fundamental component of OSC device, the construction of active layer and selection of donor and acceptor materials have been considered to make central contribution to the enhancement of the power conversion efficiency (PCE),[4-14] as they control the microstructure of morphology and even the whole efficiency of device. [15-19]

In fact, based on different active layer materials and morphology of donor/acceptor (D/A) interface, the different charge-transfer mechanisms mediated by "hot" exciton,[20, 21] "direct" excitation,[22-24] built-in and external electric field,[25-28] entropy and disorder,[29] rebound negative charge,[30] etc. have been proposed,[31-35] some of which presented contradictory conclusions and fragmentary information. For instance, just for the role of excess energy, there have been some contradictory conclusions. Tamura et al. proposed a charge-transfer mechanism promoted by vibronically hot CT states in 2013, which shows the free carrier yield ascended with the increment of excess energy but a too large excess energy is unfavorable.[21] In 2014, Sun et al. used the Ehrenfest dynamics to emphasize that a larger excess energy is more conducive to charge separation.[36] Recently, there are several reports of OSCs with high internal quantum efficiencies for charge generation with negligible excess energies.[37-39] Many of such proposals are based on highly idealized geometries of model Hamiltonian and it is not very clear if the results depend on the specific choice of the model. So what if the contradictory conclusions are sourced from different interface models built? In recent years, many researchers have devoted themselves to the study of D/A stacking effect both in experiment and theory.[40, 41] The stacking patterns of donor and acceptor have been explored from the initial distance of 3.5 Å to molecular dynamics (MD) simulation in theory.[42-44] However, as we all know, it is difficult to measure the stacking pattern at molecular level in experiment and most of the selected theoretical D/A stacking models are over-idealized. By comparison, the D/A stacking patterns obtained by MD simulations seem closer to the actual condition,[45, 46] and this technique is widely adopted to characterize the local interface morphologies of D/A blends and to understand the charge-transfer process with the analysis of electronic couplings.[44, 47-52] Meanwhile, the effect of domain size on charge-transfer mechanism of OSCs was investigated based on a large model with PCBM supercell and large polymer domains (a model constructing by 2360 and 2048 atoms for acceptor and donor, respectively) obtained by MD simulations.[53]

The goal of this work is to obtain charge-transfer mechanisms of different stacking patterns of a specific D/A model. For an active layer model simulated by MD, a statistical analysis was adopted to explore charge-transfer mechanism. And the bulk system is constructed with well-studied active layer materials dicyanovinylene (DCV)-substituted S,N-heterohexacenes-based[54-58] molecule (**D**$_{CV}$**-1**) and **C**$_{60}$ shown in Figure 1(a). Through statistical analysis on 155 D/A interfaces, we proposed a workflow visualized in Figure 1(b) to search for promising region of characteristic values for more effective D/A stacking patterns according with different charge-transfer mechanisms.

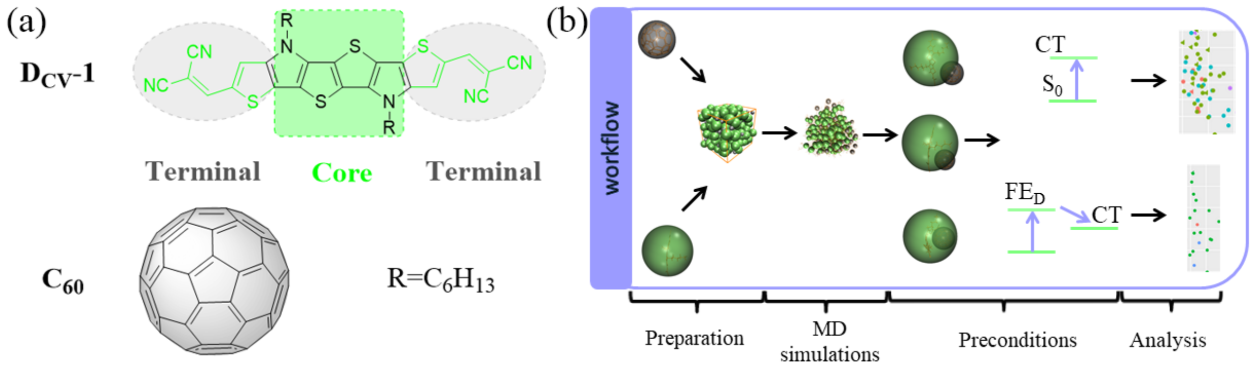

Figure 1. (a) Investigated donor molecule **D**$_{CV}$**-1** and acceptor molecule **C**$_{60}$; (Molecule **D**$_{CV}$**-1** constructed from A-D-A type including one core unit and two terminal units.) (b) Flowchart of the multi-scale simulations.

As described in Figure 2(a), the **D**$_{CV}$**-1/C**$_{60}$ interface stacking was firstly obtained by MD simulation, which is performed in Gromacs-5.1.1 software package.[59] The simulation began with a three-dimensional cubic box of sides $8 \times 8 \times 8$ nm^3 with the numbers of D/A molecules being 144/65 according to the experimental proportion.[54] The methods and details of simulation process which can give an intuitive description on the formation of **D**$_{CV}$**-1/C**$_{60}$ morphologies are exhibited in the Supporting Information (SI). Then 155 **D**$_{CV}$**-1/C**$_{60}$ stacking patterns with the centroid-to-centroid distance less than 10 Å referred to center-of mass (COM) radial distribution functions (RDFs) plotted in the SI were extracted from the final equilibration morphologies. They were further classified manually into three groups shown in Figure 2(b), namely group 1 (**C**$_{60}$ prefers to face on the center of backbone of **D**$_{CV}$**-1**), group 2 (**C**$_{60}$ tends to face on the terminal backbone of **D**$_{CV}$**-1**) and group 3 (**C**$_{60}$ locates at the edge of **D**$_{CV}$**-1**) with the assistance of configurational characteristic parameters D_C and d defined in Figure 2(c). The three groups are represented in nearly equal proportions among the 155 configurations with 50, 46, 59 instances for group 1, 2, 3 respectively.

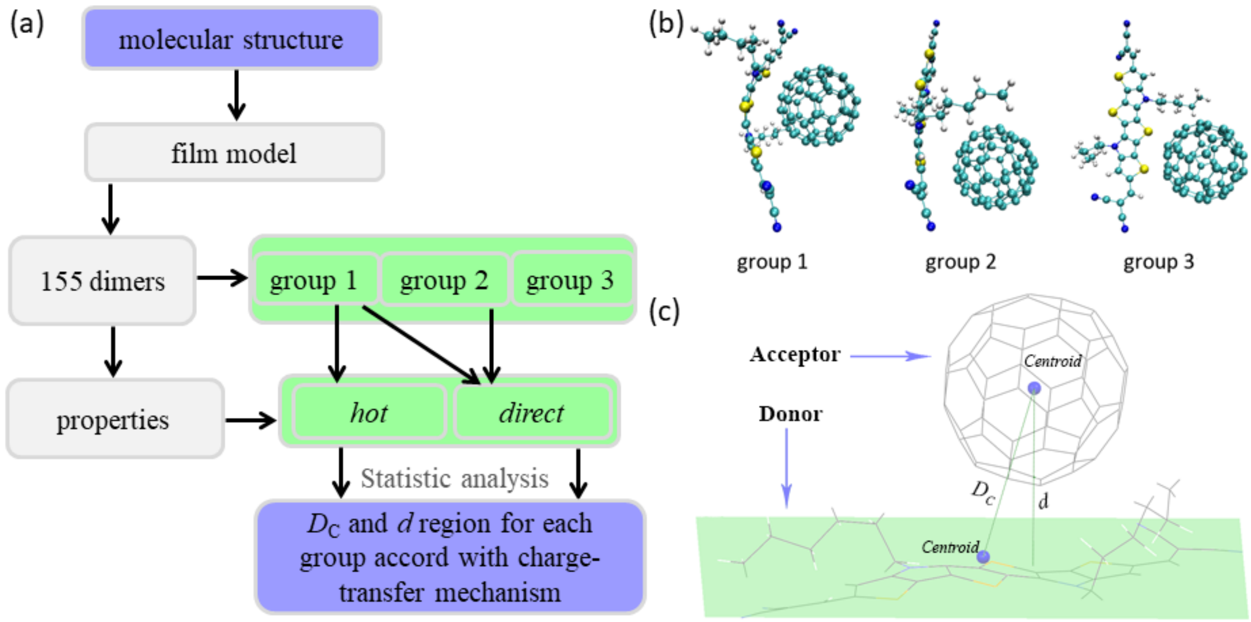

Figure 2. (a)Diagram of simulated process. (Input and output are shown in the purple frame. Manual categories are listed in the green frame); (b)Representative configurations extracted from the MD simulations for $\mathbf{D_{CV}}$**-1** and $\mathbf{C_{60}}$ molecules; (c)Schematic representation of the configurational characteristics for $\mathbf{D_{CV}}$**-1**/$\mathbf{C_{60}}$ dimer. (D_C represents the distance between centroid of donor and acceptor and d is the perpendicular distance between the centroid of acceptor and the plane of the conjugated backbone of donor.)

In order to identify the charge-transfer mechanism, we computed a number of relevant properties. Here, the counterpoised-corrected total interaction energies (E_{int}) between $\mathbf{D_{CV}}$**-1** and $\mathbf{C_{60}}$ were firstly calculated to characterize the interaction strength between donor and acceptor. The excited energies of Frenkel exciton (FE) state for donor (E_{FED}) and the lowest charge-transfer (CT) state (E_{CT}) with their respective oscillator strength f_{CT} and f_{FED} were calculated to identify their relative positions and photo-absorption strengths. Meanwhile, the energy difference between FE and CT states, namely the excess energy $E_{FE\text{-}CT}$ was also estimated for every stacking pattern aiming at distinguishing which charge-transfer mechanism it belongs to. Moreover, the electronic couplings between $\mathbf{D_{CV}}$**-1** and $\mathbf{C_{60}}$ ($V_{DA\text{-}CS}$ for charge-separation process and $V_{DA\text{-}CR}$ for charge-recombination process) were calculated considering their importance in promoting the charge-transfer ability at D/A interface using the generalized Mulliken-Hush (GMH) method[60] as described in the SI. All the calculations mentioned above were carried out at the ωb97xd/6-31G (d, p) level, which is not only suitable for the system with weak intermolecular interaction but also for the obvious charge-transfer state.[61, 62]

As a first step to analyze the large set of results, we report some interesting properties such as E_{int},

E_{FED}, E_{CT} and $E_{\mathrm{FE\text{-}CT}}$, in a scatter plot as a function of structural characteristic D_{C} in Figure 3 for 155 patterns and exhibit them in three groups. (scatter plot matrix for all computed parameters are shown in the SI.) Considering the distribution of excited state energy in Figure 3, one can notice that the stacking patterns have a relatively weak effect on the E_{FED} and a stronger effect on E_{CT}. As a consequence the excess energy $E_{\mathrm{FE\text{-}CT}}$ varies in the region of -0.9 ~ 0.7 eV largely dictated by the variation of E_{CT}. It deviates from our traditional knowledge that a fixed $E_{\mathrm{FE\text{-}CT}}$ is definite when the pair of donor and acceptor is given whether in experiment or theory, which will be focused on in this work. Moreover, making a comparison among the three groups, group 1 has lower E_{int} while group 3 seems to have higher E_{int}, which implies more stable and favorable stacking configurations for group 1. Besides, E_{CT} values of group 1 tend to be in the lower excited-energy region and those of group 3 seem to occupy in the higher excited-energy region. And higher $E_{\mathrm{FE\text{-}CT}}$ of group 1 than those of other two groups is proved by the fact that most $E_{\mathrm{FE\text{-}CT}}$ values are positive for group 1 while only three values are positive for group 2 and only two values for group 3. Hence, we infer that most of stacking patterns in group 1 are assigned to the hot mechanism (exciton dissociation via excited ("hot") electronic or vibrational levels, namely $E_{\mathrm{FE\text{-}CT}} > 0$)[20] while rare case occurs for group 2 and group 3. From the analysis above, we can find that E_{FED} does not depend too much on the packing because it is an excitation localized on the donor, while E_{CT} is influenced by the packing because greater distance between donor and acceptor increase the energy for the CT process.

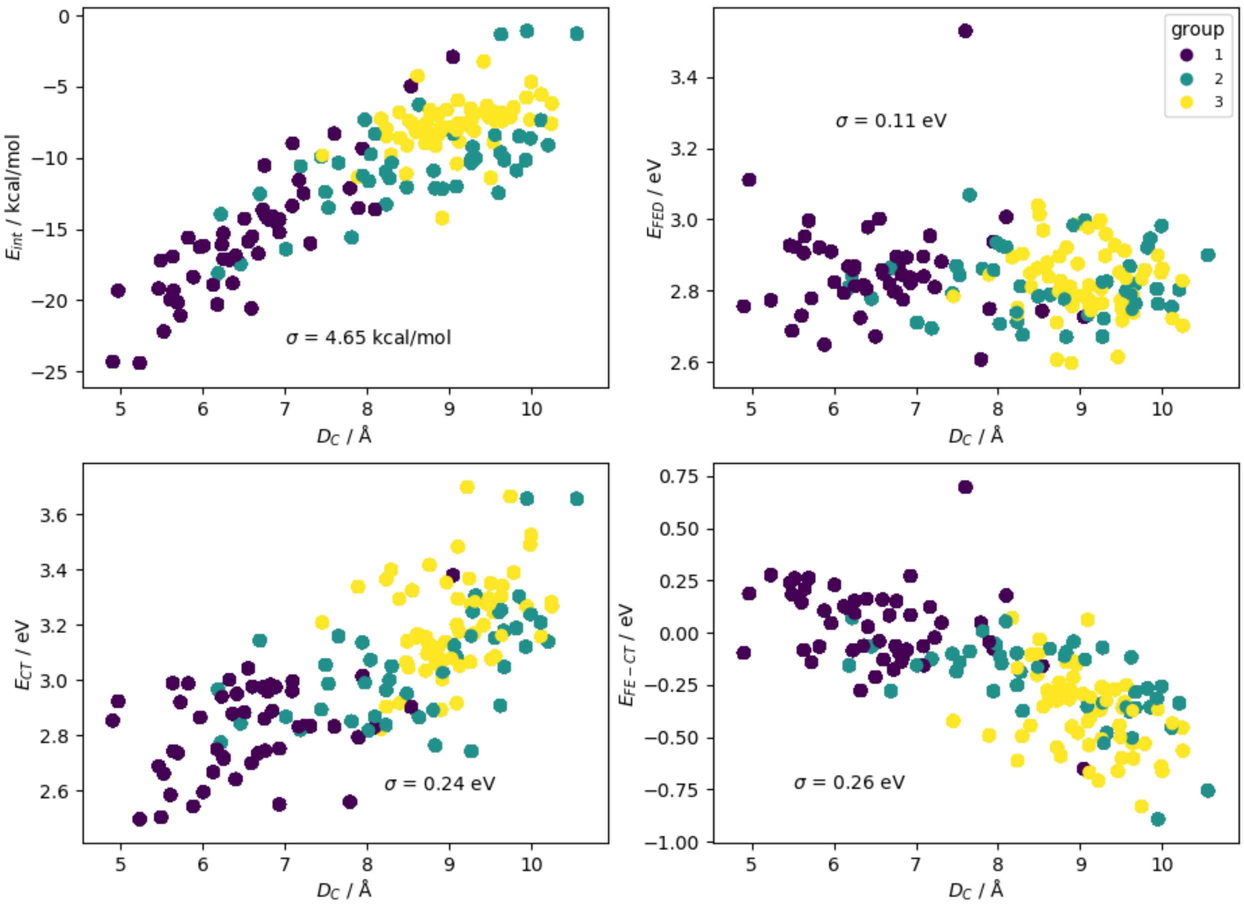

Figure 3. Scatter plot of some calculated properties as a function of D_C (E_{int}/kcal·mol^{-1}, E_{FED}/eV, E_{CT}/eV, $E_{\mathrm{FE\text{-}CT}}$/eV) of 155 dimers in different groups corresponding with average standard deviation σ.

The correlations for all calculated physical parameters are collected in Figure 4a, which shows the correlation degrees directly. From Figure 4a, largest correlation degree is easily observable between E_{CT} and $E_{\mathrm{FE\text{-}CT}}$ in light of their correlation coefficient (-0.90), which is in accordance with their linear relationship presented in scatter plot matrix in the SI. Meanwhile, the correlation coefficient between E_{int} and E_{CT} is 0.71, whose values are larger among these correlations, implying the correspondence between E_{int} and E_{CT}. Now we can infer the correlations among them, i.e., the E_{int} between donor and acceptor, which is sensitive to the stacking pattern, influences the E_{CT} and further $E_{\mathrm{FE\text{-}CT}}$. In other words, the excess energy strongly depends on the molecular stacking pattern at the interface. This is mostly influenced by the intermolecular conformation of the donor, which explains the weak correlation with other parameter. By comparison, the two parameters E_{FED} and $V_{\mathrm{DA\text{-}CS}}$ have weaker correlation with other parameters, suggesting that they are less influenced by the interface stacking pattern and may be mainly determined by our selection of active layer materials. This is weakly correlated because it is well established that the coupling is very sensitive to very small geometry change.[63]

In Figure 4b-4d, we show correlation diagrams for different groups. The relatively stronger correlation between E_{FED} and $E_{FE\text{-}CT}$ for group 1 than group 2 and group 3 may be originated from the fluctuated E_{FED} for group 1. For group 2, the electronic coupling for charge separation shows larger correlation with E_{CT}, $E_{FE\text{-}CT}$ and E_{int}, while the one for charge recombination exhibits larger correlation coefficients with f_{FED} (0.68) and f_{CT} (-0.66). These phenomena are different from the cases in group 1 and group 3, and it indicates that for the stacking patterns with $\mathbf{C_{60}}$ facing on the terminal backbone of **D**CV**-1**, stronger interaction (more negative E_{int}) is associated, as expected, with (i) lower E_{CT} (ii) higher f_{CT} and (iii) lower coupling $V_{DA\text{-}CS}$. This relation creates indirect correlations, e.g. between f_{CT} and $V_{DA\text{-}CS}$.

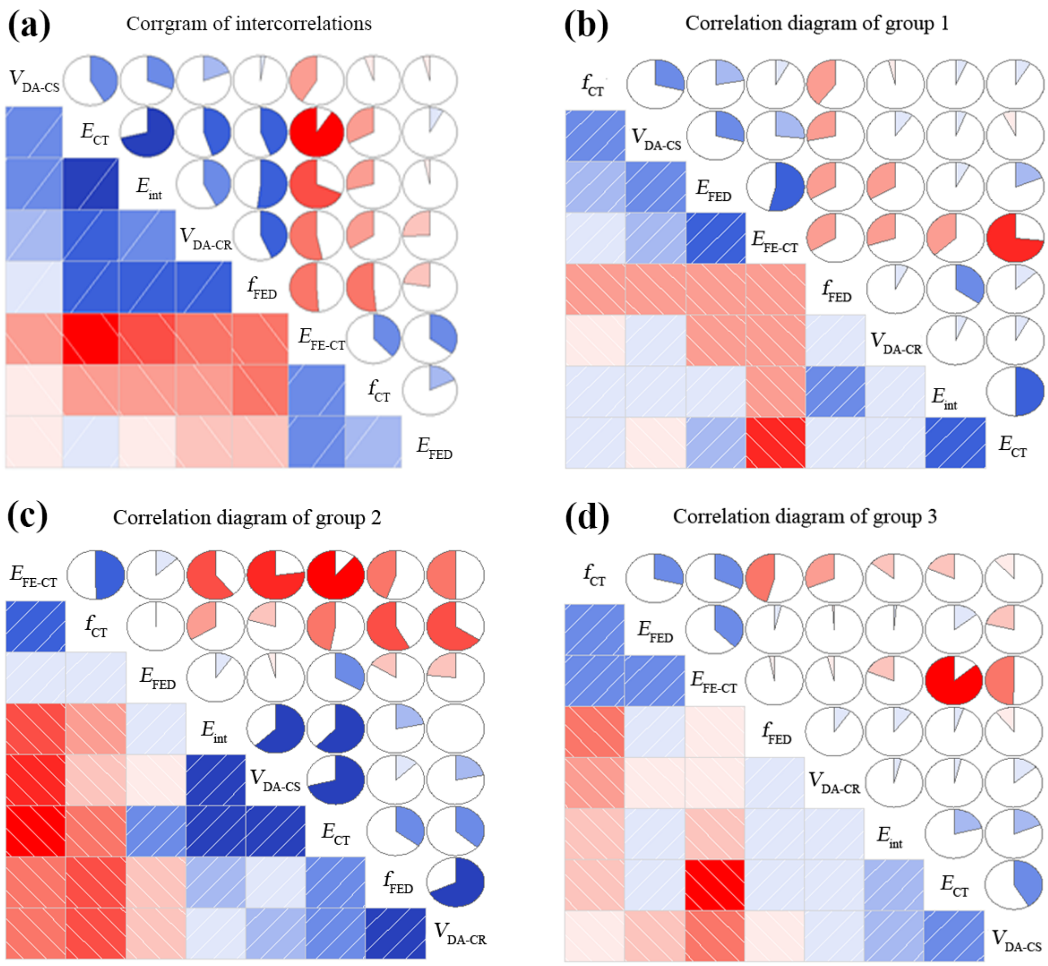

Figure 4. (a) Statistic analysis for all calculated properties (E_{int}/kcal·mol^{-1}, E_{FED}/eV, f_{FED}, E_{CT}/eV, f_{CT}, $E_{FE\text{-}CT}$/eV, $V_{DA\text{-}CS}$/eV and $V_{DA\text{-}CR}$/eV) of 155 dimers (a) and of group 1 (b), group 2 (c) and group 3 (d). (Blue and red cells indicate a positive and negative correlation, respectively, between the two variables. The darker color indicates that the variable correlation is greater. The triangular cell shows the same information with a pie chart. Correlation

coefficients between two properties larger than 0.5 are presented in the SI.)

Figure 5a plots the variation of $E_{FE\text{-}CT}$ along with characteristic values, trying to show the correlation between the energy and the structural characteristics. Combined with Figure 5b, we can see that different group tends to have distinguished region of $E_{FE\text{-}CT}$ values. A preliminary test shown in the SI was conducted to explore the effect of the excess energy $E_{FE\text{-}CT}$ on the charge-transfer mechanism by the method adopted in our previous work.[30] We can find that when the $E_{FE\text{-}CT}$ is less than zero, as the $E_{FE\text{-}CT}$ increases, the maximum time-averaged outgoing charge $\bar{P}_{\text{out}}$ increases slowly at first and then rises substantially. When $E_{FE\text{-}CT}$ values are approaching zero, more and more charges in bound-CT states are separated into outgoing charges. When $E_{FE\text{-}CT}$ is greater than zero, $\bar{P}_{\text{out}}$ decreases drastically as $E_{FE\text{-}CT}$ increases. This is because the systems adopt hot mechanism, and the generated charges in bound-CT state are small. Considering that $\bar{P}_{\text{out}}$ can reach its peak when $E_{FE\text{-}CT}$ is close to zero, we can imagine that the appearance of Frenkel exciton state and CT state as a hybrid state will facilitate charge separation. It is in accordance with our another work[64] that the hybrid state is favorable to improve charge dissociation.

In order to provide a specific distinction between charge-transfer mechanisms for the three groups, the position distributions along with the corresponding charge-transfer mechanisms, namely hot mechanism and direct mechanism (charge dissociation can take place directly into charge), are detailed in Figure 5c-5d. It can be seen from Figure 5b that both D_C and d for group 1 are mostly located in the range of (5.0 Å, 7.5 Å), while for group 2, D_C are relatively larger with the same range of d with group 1, and for group 3, D_C are also large with d varying widely (0~9 Å). Overall, when D_C is smaller than 8 Å, most configurations belong to group 1, and more stacking patterns of group 1 are assigned to the hot mechanism with reference to Figure 5c, which only considers lower E_{int}, larger $V_{DA\text{-}CS}$ and smaller $V_{DA\text{-}CR}$ (The relative lower or larger value are selected on the basis of the distribution of data. According to the distance between two adjacent points, the data is arranged in order from small to large. If the distance between two adjacent points is relatively large, the middle of these two points is the split point.) for hot mechanism. We know that effective charge dissociation needs larger $V_{DA\text{-}CS}$ and smaller $V_{DA\text{-}CR}$. The corresponding promising region (D_C = (5.5, 7.8) and d = (6.2, 6.6)) for hot mechanism in group 1 are presented in the SI. While for group 2 and group 3, hot mechanism is not considered because the majority of negative $E_{FE\text{-}CT}$ values are in both groups. In comparison, the stacking patterns assigned to direct mechanism show a larger proportion according to the dense distribution in Figure 5d, whereas, the position distributions with effective charge dissociations are still concentrated at smaller intermolecular distance. The promising regions for direct mechanism of group 1 (D_C = (5.5, 7.4) and d = (6.0, 6.7)) and group 2 (D_C = (7.0, 9.0) and d = (6.0, 7.0)) are shown in the SI. Therefore, we get the conclusion that the hot mechanism mainly appears in group 1, while direct mechanism mainly appears in group 1 and group 2, and more stacking patterns in group 3 behave ineffective charge dissociations considering their smaller $V_{DA\text{-}CS}$ and nearly zero f_{CT}.

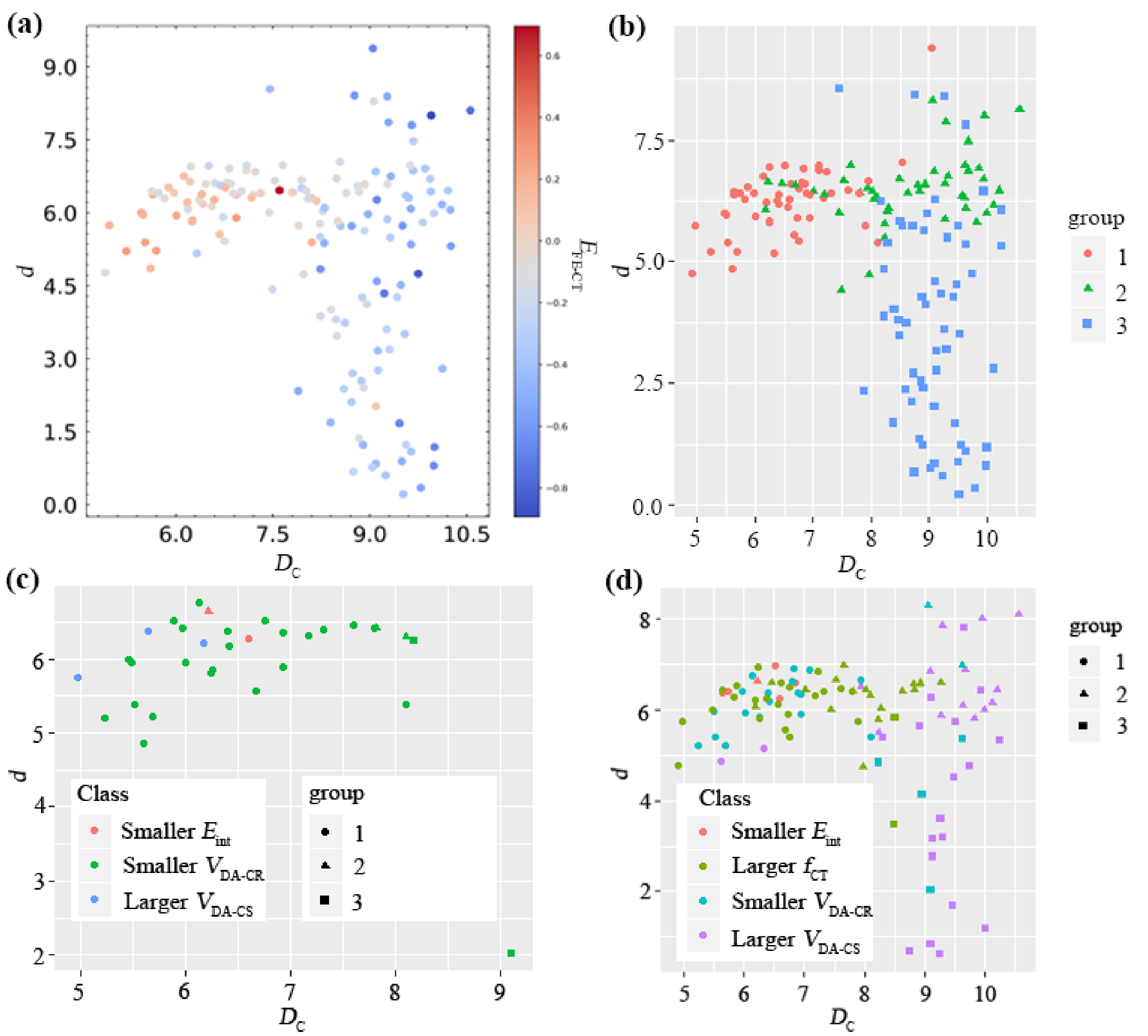

Figure 5. (a) Distribution of $E_{FE\text{-}CT}$ along with D_C and d for the dimers; (b) Distributions of D_C and d for all of 155 dimers; (c) Distributions of D_C and d for the dimers with hot mechanism (only consider $E_{FE\text{-}CT} > 0$). Region D_C = (5.5, 8.0) (Å) and d = (5.5, 6.5) (Å) is promising; (d) Distributions of D_C and d for the dimers with direct mechanism. Region D_C = (5.0, 8.0) (Å) and d = (5.0, 7.0) (Å) is promising.

In conclusion, we performed a statistical analysis on the key parameters related to the charge dissociation in an active layer model trying to search possible charge-transfer mechanisms. We find that different charge dissociation mechanisms become more likely depending on the packing of the D/A pair. A hot exciton mechanism is the most likely to occur when the acceptor and donor are the closest with acceptor lying on the central of donor (in about one third of configurations). While the packings for acceptor faced on the donor molecule could have a strong propensity to have direct excitation of the charge-transfer state. As for those acceptor edged on the donor are hardly satisfied with either hot or direct mechanism. In addition, the quantum dynamics simulation suggests that when the excess energies come close to zero, the separation charge yield is approaching the peak. This work demonstrates the importance of considering large sample of intermolecular geometries to draw useful conclusions on the actual charge dissociation mechanism.

Aknowledgements

The authors gratefully acknowledge financial support from National Natural Science Foundation of China (21771035, 21663011), the Fundamental Research Funds for the Central Universities (2412018ZD006). We really thank Ph. D. candidate Qiang Zhu in Nanjing University for suggestions in the MD simulations and Miss Shi-Yan Zheng for fruitful discussions in the statistical analysis.

References

1. Yu, G.; Gao, J.; Hummelen, J. C.; Wudl, F.; Heeger, A. J., Polymer Photovoltaic Cells: Enhanced Efficiencies via a Network of Internal Donor-Acceptor Heterojunctions. *Science* **1995,** *270* (5243), 1789-1791.
2. Heeger, A. J., 25th anniversary article: Bulk heterojunction solar cells: understanding the mechanism of operation. *Adv. Mater.* **2014,** *26* (1), 10-27.
3. Zhang, G.; Zhao, J.; Chow, P. C. Y.; Jiang, K.; Zhang, J.; Zhu, Z.; Zhang, J.; Huang, F.; Yan, H., Nonfullerene Acceptor Molecules for Bulk Heterojunction Organic Solar Cells. *Chem. Rev.* **2018,** *118* (7), 3447-3507.
4. Olivares-Amaya, R.; Amador-Bedolla, C.; Hachmann, J.; Atahan-Evrenk, S.; Sánchez-Carrera, R. S.; Vogt, L.; Aspuru-Guzik, A., Accelerated computational discovery of high-performance materials for organic photovoltaics by means of cheminformatics. *Energy Environ. Sci.* **2011,** *4* (12).
5. Hachmann, J.; Olivares-Amaya, R.; Jinich, A.; Appleton, A. L.; Blood-Forsythe, M. A.; Seress, L. R.; Román-Salgado, C.; Trepte, K.; Atahan-Evrenk, S.; Er, S.; Shrestha, S.; Mondal, R.; Sokolov, A.; Bao, Z.; Aspuru-Guzik, A., Lead candidates for high-performance organic photovoltaics from high-throughput quantum chemistry – the Harvard Clean Energy Project. *Energy Environ. Sci.* **2014,** *7* (2), 698-704.
6. Sahu, H.; Yang, F.; Ye, X.; Ma, J.; Fang, W.; Ma, H., Designing promising molecules for organic solar cells

via machine learning assisted virtual screening. *J. Mater. Chem. A* **2019,** *7* (29), 17480-17488.

7. Yuan, J.; Zhang, Y.; Zhou, L.; Zhang, G.; Yip, H.-L.; Lau, T.-K.; Lu, X.; Zhu, C.; Peng, H.; Johnson, P. A.; Leclerc, M.; Cao, Y.; Ulanski, J.; Li, Y.; Zou, Y., Single-Junction Organic Solar Cell with over 15% Efficiency Using Fused-Ring Acceptor with Electron-Deficient Core. *Joule* **2019,** *3* (4), 1140-1151.

8. Green, M. A.; Hishikawa, Y.; Dunlop, E. D.; Levi, D. H.; Hohl-Ebinger, J.; Ho-Baillie, A. W. Y., Solar cell efficiency tables (version 52). *Progress in Photovoltaics: Research and Applications* **2018,** *26* (7), 427-436.

9. Yao, H.; Ye, L.; Zhang, H.; Li, S.; Zhang, S.; Hou, J., Molecular Design of Benzodithiophene-Based Organic Photovoltaic Materials. *Chem. Rev.* **2016,** *116* (12), 7397-457.

10. Fan, B.; Zhang, D.; Li, M.; Zhong, W.; Zeng, Z.; Ying, L.; Huang, F.; Cao, Y., Achieving over 16% efficiency for single-junction organic solar cells. *Sci. China Chem.* **2019,** *62* (6), 746-752.

11. Hou, J.; Inganas, O.; Friend, R. H.; Gao, F., Organic solar cells based on non-fullerene acceptors. *Nat. Mater.* **2018,** *17* (2), 119-128.

12. Zhang, Y.; Kan, B.; Sun, Y.; Wang, Y.; Xia, R.; Ke, X.; Yi, Y. Q.; Li, C.; Yip, H. L.; Wan, X.; Cao, Y.; Chen, Y., Nonfullerene Tandem Organic Solar Cells with High Performance of 14.11. *Adv. Mater.* **2018,** *30* (18), e1707508.

13. Zhang, S.; Qin, Y.; Zhu, J.; Hou, J., Over 14% Efficiency in Polymer Solar Cells Enabled by a Chlorinated Polymer Donor. *Adv. Mater.* **2018,** *30* (20), e1800868.

14. Meng, L.; Zhang, Y.; Wan, X.; Li, C.; Zhang, X.; Wang, Y.; Ke, X.; Xiao, Z.; Ding, L.; Xia, R.; Yip, H.-L.; Cao, Y.; Chen, Y., Organic and solution-processed tandem solar cells with 17.3% efficiency. *Science* **2018,** *361* (6407), 1094.

15. Zhu, L.; Zhang, M.; Zhou, G.; Hao, T.; Xu, J.; Wang, J.; Qiu, C.; Prine, N.; Ali, J.; Feng, W.; Gu, X.; Ma, Z.; Tang, Z.; Zhu, H.; Ying, L.; Zhang, Y.; Liu, F., Efficient Organic Solar Cell with 16.88% Efficiency Enabled by Refined Acceptor Crystallization and Morphology with Improved Charge Transfer and Transport Properties. *Adv. Energy Mater.* **2020**, 1904234.

16. Hamid, Z.; Wadsworth, A.; Rezasoltani, E.; Holliday, S.; Azzouzi, M.; Neophytou, M.; Guilbert, A. A. Y.; Dong, Y.; Little, M. S.; Mukherjee, S.; Herzing, A. A.; Bristow, H.; Kline, R. J.; DeLongchamp, D. M.; Bakulin, A. A.; Durrant, J. R.; Nelson, J.; McCulloch, I., Influence of Polymer Aggregation and Liquid Immiscibility on Morphology Tuning by Varying Composition in PffBT4T-2DT/Nonfullerene Organic Solar Cells. *Adv. Energy Mater.* **2020,** *10* (8), 1903248.

17. Yi, X.; Peng, Z.; Xu, B.; Seyitliyev, D.; Ho, C. H. Y.; Danilov, E. O.; Kim, T.; Reynolds, J. R.; Amassian, A.; Gundogdu, K.; Ade, H.; So, F., Critical Role of Polymer Aggregation and Miscibility in Nonfullerene-Based Organic Photovoltaics. *Adv. Energy Mater.* **2020,** *10* (8), 1902430.

18. Yi, N.; Ai, Q.; Zhou, W.; Huang, L.; Zhang, L.; Xing, Z.; Li, X.; Zeng, J.; Chen, Y., Miscibility Matching and Bimolecular Crystallization Affording High-Performance Ternary Nonfullerene Solar Cells. *Chem. Mater.* **2019,** *31* (24), 10211-10224.

19. Zhou, Z.; Liu, W.; Zhou, G.; Zhang, M.; Qian, D.; Zhang, J.; Chen, S.; Xu, S.; Yang, C.; Gao, F.; Zhu, H.; Liu, F.; Zhu, X., Subtle Molecular Tailoring Induces Significant Morphology Optimization Enabling over 16% Efficiency Organic Solar Cells with Efficient Charge Generation. *Adv. Mater.* **2020,** *32* (4), 1906324.

20. Brédas, J.-L.; Norton, J. E.; Cornil, J.; Coropceanu, V., Molecular Understanding of Organic Solar Cells: The Challenges. *Acc. Chem. Res.* **2009,** *42* (11), 1691-1699.

21. Tamura, H.; Burghardt, I., Ultrafast charge separation in organic photovoltaics enhanced by charge delocalization and vibronically hot exciton dissociation. *J. Am. Chem. Soc.* **2013,** *135* (44), 16364-7.

22. Ran, N. A.; Love, J. A.; Takacs, C. J.; Sadhanala, A.; Beavers, J. K.; Collins, S. D.; Huang, Y.; Wang, M.; Friend, R. H.; Bazan, G. C.; Nguyen, T. Q., Harvesting the Full Potential of Photons with Organic Solar Cells. *Adv.*

Mater. **2016,** *28* (7), 1482-8.
23. Lee, J.; Vandewal, K.; Yost, S. R.; Bahlke, M. E.; Goris, L.; Baldo, M. A.; Manca, J. V.; Van Voorhis, T., Charge Transfer State Versus Hot Exciton Dissociation in Polymer−Fullerene Blended Solar Cells. *J. Am. Chem. Soc.* **2010,** *132* (34), 11878-11880.
24. Ma, H.; Troisi, A., Direct Optical Generation of Long-Range Charge-Transfer States in Organic Photovoltaics. *Adv. Mater.* **2014,** *26* (35), 6163-6167.
25. Yao, H.; Qian, D.; Zhang, H.; Qin, Y.; Xu, B.; Cui, Y.; Yu, R.; Gao, F.; Hou, J., Critical Role of Molecular Electrostatic Potential on Charge Generation in Organic Solar Cells. *Chin. J. Chem.* **2018,** *36* (6), 491-494.
26. Weu, A.; Hopper, T. R.; Lami, V.; Kreß, J. A.; Bakulin, A. A.; Vaynzof, Y., Field-Assisted Exciton Dissociation in Highly Efficient PffBT4T-2OD:Fullerene Organic Solar Cells. *Chem. Mater.* **2018,** *30* (8), 2660-2667.
27. Yao, H.; Cui, Y.; Qian, D.; Ponseca, C. S., Jr.; Honarfar, A.; Xu, Y.; Xin, J.; Chen, Z.; Hong, L.; Gao, B.; Yu, R.; Zu, Y.; Ma, W.; Chabera, P.; Pullerits, T.; Yartsev, A.; Gao, F.; Hou, J., 14.7% Efficiency Organic Photovoltaic Cells Enabled by Active Materials with a Large Electrostatic Potential Difference. *J. Am. Chem. Soc.* **2019,** *141* (19), 7743-7750.
28. Yan, Y.; Song, L.; Shi, Q., Understanding the free energy barrier and multiple timescale dynamics of charge separation in organic photovoltaic cells. *J. Chem. Phys.* **2018,** *148* (8), 084109.
29. Hood, S. N.; Kassal, I., Entropy and Disorder Enable Charge Separation in Organic Solar Cells. *J. Phys. Chem. Lett.* **2016,** *7* (22), 4495-4500.
30. Geng, Y.; Lee, M. H.; Troisi, A., Effect of Infrared Pulse Excitation on the Bound Charge-Transfer State of Photovoltaic Interfaces. *J. Phys. Chem. Lett.* **2017,** *8* (19), 4872-4877.
31. Joseph, S.; Ravva, M. K.; Bredas, J. L., Charge-Transfer Dynamics in the Lowest Excited State of a Pentacene-Fullerene Complex: Implications for Organic Solar Cells. *J. Phys. Chem. Lett.* **2017,** *8* (20), 5171-5176.
32. Bakulin, A. A.; Dimitrov, S. D.; Rao, A.; Chow, P. C.; Nielsen, C. B.; Schroeder, B. C.; McCulloch, I.; Bakker, H. J.; Durrant, J. R.; Friend, R. H., Charge-Transfer State Dynamics Following Hole and Electron Transfer in Organic Photovoltaic Devices. *J. Phys. Chem. Lett.* **2013,** *4* (1), 209-15.
33. Eisner, F. D.; Azzouzi, M.; Fei, Z.; Hou, X.; Anthopoulos, T. D.; Dennis, T. J. S.; Heeney, M.; Nelson, J., Hybridization of Local Exciton and Charge-Transfer States Reduces Nonradiative Voltage Losses in Organic Solar Cells. *J. Am. Chem. Soc.* **2019,** *141* (15), 6362-6374.
34. Han, G.; Yi, Y., Local Excitation/Charge-Transfer Hybridization Simultaneously Promotes Charge Generation and Reduces Nonradiative Voltage Loss in Nonfullerene Organic Solar Cells. *J. Phys. Chem. Lett.* **2019,** *10* (11), 2911-2918.
35. Zheng, Z.; Tummala, N. R.; Fu, Y. T.; Coropceanu, V.; Bredas, J. L., Charge-Transfer States in Organic Solar Cells: Understanding the Impact of Polarization, Delocalization, and Disorder. *ACS Appl. Mater. Interfaces* **2017,** *9* (21), 18095-18102.
36. Sun, Z.; Stafström, S., Dynamics of charge separation at an organic donor-acceptor interface. *Phys. Rev. B* **2014,** *90* (11).
37. Vandewal, K.; Albrecht, S.; Hoke, E. T.; Graham, K. R.; Widmer, J.; Douglas, J. D.; Schubert, M.; Mateker, W. R.; Bloking, J. T.; Burkhard, G. F.; Sellinger, A.; Frechet, J. M.; Amassian, A.; Riede, M. K.; McGehee, M. D.; Neher, D.; Salleo, A., Efficient charge generation by relaxed charge-transfer states at organic interfaces. *Nat. Mater.* **2014,** *13* (1), 63-8.
38. Menke, S. M.; Cheminal, A.; Conaghan, P.; Ran, N. A.; Greehnam, N. C.; Bazan, G. C.; Nguyen, T. Q.; Rao, A.; Friend, R. H., Order enables efficient electron-hole separation at an organic heterojunction with a small energy loss. *Nat. Commun.* **2018,** *9* (1), 277.
39. Liu, J.; Chen, S.; Qian, D.; Gautam, B.; Yang, G.; Zhao, J.; Bergqvist, J.; Zhang, F.; Ma, W.; Ade, H.; Inganäs, O.; Gundogdu, K.; Gao, F.; Yan, H., Fast charge separation in a non-fullerene organic solar cell with a

small driving force. *Nat. Energy* **2016,** *1* (7).

40. Zhou, R.; Jiang, Z.; Yang, C.; Yu, J.; Feng, J.; Adil, M. A.; Deng, D.; Zou, W.; Zhang, J.; Lu, K.; Ma, W.; Gao, F.; Wei, Z., All-small-molecule organic solar cells with over 14% efficiency by optimizing hierarchical morphologies. *Nat. Commun.* **2019,** *10* (1), 5393.

41. Jakowetz, A. C.; Bohm, M. L.; Zhang, J.; Sadhanala, A.; Huettner, S.; Bakulin, A. A.; Rao, A.; Friend, R. H., What Controls the Rate of Ultrafast Charge Transfer and Charge Separation Efficiency in Organic Photovoltaic Blends. *J. Am. Chem. Soc.* **2016,** *138* (36), 11672-9.

42. Pan, Q.-Q.; Li, S.-B.; Wu, Y.; Geng, Y.; Zhang, M.; Su, Z.-M., Exploring more effective polymer donors for the famous non-fullerene acceptor ITIC in organic solar cells by increasing electron-withdrawing ability. *Org. Electron.* **2018,** *53*, 308-314.

43. Zhao, Z.-W.; Duan, Y.-C.; Pan, Q.-Q.; Gao, Y.; Wu, Y.; Geng, Y.; Zhao, L.; Zhang, M.; Su, Z.-M., A probe into underlying factors affecting utrafast charge transfer at Donor/IDIC interface of all-small-molecule nonfullerene organic solar cells. *J. Photoch. Photobio. A* **2019,** *375*, 1-8.

44. Han, G.; Yi, Y.; Shuai, Z., From Molecular Packing Structures to Electronic Processes: Theoretical Simulations for Organic Solar Cells. *Adv. Energy Mater.* **2018,** *8* (28), 1702743.

45. Long, G.; Li, A.; Shi, R.; Zhou, Y.-C.; Yang, X.; Zuo, Y.; Wu, W.-R.; Jeng, U. S.; Wang, Y.; Wan, X.; Shen, P.; Zhang, H.-L.; Yan, T.; Chen, Y., The Evidence for Fullerene Aggregation in High-Performance Small-Molecule Solar Cells by Molecular Dynamics Simulation. *Adv. Energy Mater.* **2015,** *1* (11).

46. Cheung, D. L.; Troisi, A., Theoretical Study of the Organic Photovoltaic Electron Acceptor PCBM: Morphology, Electronic Structure, and Charge Localization. *J. Phys. Chem. C* **2010,** *114* (48), 20479-20488.

47. Liu, T.; Cheung, D. L.; Troisi, A., Structural variability and dynamics of the P3HT/PCBM interface and its effects on the electronic structure and the charge-transfer rates in solar cells. *Phys. Chem. Chem. Phys.* **2011,** *13* (48), 21461-21470.

48. Fu, Y.-T.; Risko, C.; Brédas, J.-L., Intermixing at the Pentacene-Fullerene Bilayer Interface: A Molecular Dynamics Study. *Adv. Mater.* **2013,** *25* (6), 878-882.

49. D'Avino, G.; Mothy, S.; Muccioli, L.; Zannoni, C.; Wang, L.; Cornil, J.; Beljonne, D.; Castet, F., Energetics of Electron–Hole Separation at P3HT/PCBM Heterojunctions. *J. Phys. Chem. C* **2013,** *117* (25), 12981-12990.

50. Do, K.; Ravva, M. K.; Wang, T.; Brédas, J.-L., Computational Methodologies for Developing Structure–Morphology–Performance Relationships in Organic Solar Cells: A Protocol Review. *Chem. Mater.* **2017,** *29* (1), 346-354.

51. Shimazaki, T.; Tashiro, M.; Nakajima, T., Theoretical study on mesoscopic-size impurity effects in the charge separation process of organic photocells. *Phys. Chem. Chem. Phys.* **2018,** *20* (21), 14846-14854.

52. McMahon, D. P.; Cheung, D. L.; Troisi, A., Why Holes and Electrons Separate So Well in Polymer/Fullerene Photovoltaic Cells. *J. Phys. Chem. Lett* **2011,** *2* (21), 2737-2741.

53. Boschetto, G.; Krompiec, M.; Skylaris, C.-K., Insights into the Charge-Transfer Mechanism of Organic Photovoltaics: Effect of Domain Size. *J. Phys. Chem. C* **2018,** *122* (30), 17024-17034.

54. Wetzel, C.; Mishra, A.; Mena-Osteritz, E.; Walzer, K.; Pfeiffer, M.; Bäuerle, P., Development of strongly absorbing S,N-heterohexacene-based donor materials for efficient vacuum-processed organic solar cells. *J. Mater. Chem. C* **2016,** *4* (17), 3715-3725.

55. Chung, C. L.; Chen, H. C.; Yang, Y. S.; Tung, W. Y.; Chen, J. W.; Chen, W. C.; Wu, C. G.; Wong, K. T., S,N-Heteroacene-Based Copolymers for Highly Efficient Organic Field Effect Transistors and Organic Solar Cells: Critical Impact of Aromatic Subunits in the Ladder pi-System. *ACS Appl. Mater. Interfaces* **2018,** *10* (7), 6471-6483.

56. Huang, C.; Liao, X.; Gao, K.; Zuo, L.; Lin, F.; Shi, X.; Li, C.-Z.; Liu, H.; Li, X.; Liu, F.; Chen, Y.; Chen, H.; Jen, A. K. Y., Highly Efficient Organic Solar Cells Based on S,N-Heteroacene Non-Fullerene Acceptors. *Chem. Mater.* **2018,** *30* (15), 5429-5434.

57. Biswas, S.; Pramanik, A.; Pal, S.; Sarkar, P., A Theoretical Perspective on the Photovoltaic Performance of S,N-Heteroacenes: An Even–Odd Effect on the Charge Separation Dynamics. *J. Phys. Chem. C* **2017,** *121* (5), 2574-2587.
58. Geng, Y.; Tang, A.; Tajima, K.; Zeng, Q.; Zhou, E., Conjugated materials containing dithieno[3,2-b:2′,3′-d]pyrrole and its derivatives for organic and hybrid solar cell applications. *J. Mater. Chem. A* **2019,** *7* (1), 64-96.
59. Hess, B.; Kutzner, C.; van der Spoel, D.; Lindahl, E., GROMACS 4: Algorithms for Highly Efficient, Load-Balanced, and Scalable Molecular Simulation. *J. Chem. Theory Comput.* **2008,** *4* (3), 435-447.
60. Voityuk, A. A., Estimation of electronic coupling in pi-stacked donor-bridge-acceptor systems: correction of the two-state model. *J. Chem. Phys.* **2006,** *124* (6), 64505.
61. Chai, J. D.; Head-Gordon, M., Long-range corrected hybrid density functionals with damped atom-atom dispersion corrections. *Phys. Chem. Chem. Phys.* **2008,** *10* (44), 6615-20.
62. Ravva, M. K.; Wang, T.; Brédas, J.-L., Nature of the Binding Interactions between Conjugated Polymer Chains and Fullerenes in Bulk Heterojunction Organic Solar Cells. *Chem. Mater.* **2016,** *28* (22), 8181-8189.
63. Troisi, A.; Orlandi, G., Hole Migration in DNA: a Theoretical Analysis of the Role of Structural Fluctuations. *J. Phys. Chem. B* **2002,** *106* (8), 2093-2101.
64. Zhao, Z.-W.; Pan, Q.-Q.; Geng, Y.; Wu, Y.; Zhao, L.; Zhang, M.; Su, Z.-M., Theoretical Insight into Multiple Charge-Transfer Mechanisms at the P3HT/Nonfullerenes Interface in Organic Solar Cells. *ACS Sustain. Chem. Eng.* **2019,** *7* (24), 19699-19707.